Journal of Materials Chemistry A



PAPER



Cite this: J. Mater. Chem. A, 2024, 12, 7943

Energy harvesting and electricity production through dissolved carbon dioxide by connecting two form-stable phase change materials†

Herein, we report a new solar energy harvesting approach by connecting two form-stable phase change materials in a moist environment with dissolved carbon dioxide (CO₂). Recently, a smart and creative energy harvesting concept has emerged by using form-stable phase change material (PCM) composites without any thermoelectric device. In that approach, the two form-stable PCM composites must have different electrical resistivities and phase transition temperatures based on the Seebeck effect. In this study, there is no need to make the PCM composite an electrical conductor. Instead, we propose the usage of different relative humidities on the surfaces of the two connected PCM composites and dissolved carbon dioxide as the moving ions to produce electricity. For this purpose, we synthesized and 3D printed a hydrophilic shape memory vitrimer (SMV) container as the supporting material. By infiltrating two types of PCMs into the SMV supporting container, two types of PCM composites were obtained. By changing the surface moisture content and the concentration of dissolved CO2, PCM composites with different electrical resistivities were realized. Comprehensive characterization studies were conducted on the synthesized SMV, PCMs, and PCM composites. The effect of the relative humidity and CO₂ concentrations on the electrical energy outputs was investigated. Several groups or assembly were further investigated. It was found that an assembly made of SMV supported 1tetradecanol with 70% relative humidity and SMV supported polyethylene glycol with 90% relative humidity at 700 ppm and 1200 ppm CO₂ concentrations preformed the best. The voltage and current outputs were about 2.73 mV and 500 nA during the light-on/off process, respectively. Numerical simulation was also conducted, which largely confirmed the experimental results. This study shows that greenhouse gases can be effectively employed to harvest energy. It is believed that this study provided new opportunities for clean energy harvesting.

Received 5th November 2023 Accepted 18th February 2024

DOI: 10.1039/d3ta06766a

rsc.li/materials-a

1. Introduction

Nowadays, energy harvesting is one of the most important issues because of the depletion of fossil fuels and climate change due to the greenhouse effect. The daily consumption of fossil fuel leads to environmental pollution and climate change. Replacement of fossil fuels by clean and renewable energy is indispensable to both mitigate the energy crisis and reduce environmental destruction.^{1,2} To achieve this objective, clean energy harvesting is a current mission in both academic and industrial research. Solar energy is an abundant clean energy source that can contribute to mitigating the energy crisis effectively.^{3,4} In theory, the amount of solar energy reaching the

nized as such a material.

A PCM exhibits a high heat of fusion and can absorb and release a large amount of thermal energy during the phase

storage (TES) capacity. Phase change material (PCM) is recog-

Earth for one hour is equal to one year's energy consumption of

the world.⁵ Therefore, utilization of solar energy is quite important to provide adequate power sources for energy

consumption.6,7 Harnessing sunlight to generate electrical

energy has been done by solar cells.8,9 This is related to a solar

photovoltaic (PV) system which can convert sunlight into usable electricity directly. Moreover, solar energy can be utilized for

solar heating and cooling applications to generate electrical

energy according to the Seebeck effect. ^{12,13} A solar energy device results in solar-to-electrical energy harvesting due to the presence of a temperature difference between the two sides of the device. ^{14,15} While solar energy devices, especially those based on the Seebeck effect, have numerous advantages, they must accumulate sunlight and store it as thermal energy for a long time. Increasing the duration of solar energy harvesting requires a suitable substance with a high thermal energy

^aDepartment of Mechanical and Industrial Engineering, Louisiana State University, Baton Rouge, LA 70803, USA

^bDepartment of Mechanical Engineering, Southern University, A &M College, Baton Rouge, LA 70813, USA. E-mail: lguoqi1@lsu.edu

transition process due to the high latent heat and thermal density. 16,17 When a PCM undergoes solid-liquid phase change, the intermolecular structures are disrupted, which demands a lot of energy to break the intermolecular bonds. 18,19 Thus, the PCM shows a nearly isothermal state when it changes from a solid to a liquid and stores a plenty of thermal energy effectively. 20,21 Similar to the liquid to solid crystallization process, intermolecular bonds form when the stored energy starts to release. Therefore, the reversible phase change can produce a stable temperature difference for harvesting thermoelectric energy.^{22,23} Because of high latent heat, appropriate phase transition temperature, and excellent chemical stability, solidliquid PCMs have been extensively utilized for numerous applications through high latent heat thermal energy storage (LHTES).^{24,25} However, the leakage problem during the solid to liquid phase change restricts the widespread utilization of pure PCMs since it is difficult to prevent the initial solid state from leaking during the melting process.^{26,27} It requires some kind of supporting materials to prevent leakage. To this end, microencapsulation and vacuum impregnation methods have been adopted to fabricate form-stable PCM composites.

Recently, polyaniline (PANI) and poly(methyl methacrylate) (PMMA) have been used as supporting materials to fabricate microencapsulated PCM composites.28,29 This type of encapsulated microsphere structure can maintain the PCM without any leakage during the phase transition process. For the sake of increasing the weight fraction of the pure PCM, porous supporting materials have been selected and pure PCMs have been infiltrated into the pore volume to obtain a form-stable PCM composite.30,31 Considering that carbon based materials can absorb sunlight efficiently, a graphene aerogel supported PCM composite has also been utilized for constructing a solar-toelectrical power generator and produced a stable and continuous electrical energy output during the light-on/-off process.32,33 In addition, two types of PCM composites with different phase transition temperatures have been connected onto each side of a power generator to generate electrical energy during the heating and cooling processes.34,35 The working condition of this model is close to that for practical applications, which makes it possible to generate electrical energy merely with the change in external temperatures. Although excellent studies have been reported recently by connecting PCM composites with energy harvesting devices to produce electrical energy, it remains a limitation for further utilization because energy harvesting devices are costly.

Herein, we propose the elimination of energy harvesting devices by directly connecting two types of PCM composites with different electrical conductivities and different phase change temperatures. It works with the Seebeck effect. In particular, we propose the production of the different electrical conductivities by changing the surface humidity of the PCM composites with different concentrations of dissolved carbon dioxide (CO_2) .

Unlike previous studies, in this study, we propose the usage of a 3D printed hydrophilic shape memory vitrimer (SMV) or vitrimer for short as the supporting material to prepare form-stable PCM composites. One reason for using SMV to

manufacture the supporting container is that under cyclic thermal loading, fatigue failure may occur in the container of the form-stable PCM composites. The cracks, if not healed, will lead to leaking of the PCM. As a result, the energy harvesting assembly will stop working. Furthermore, at the end of the service life, one may want to recycle the container and the PCM to make the system sustainable. SMVs, as chemically crosslinked thermoset polymers, have outstanding mechanical properties, shape memory effect, self-healing capability, and recyclability.36,37 Particularly, a combination of the shape memory effect and intrinsic self-healing capability can help heal wider opened cracks per the biomimetic close-then-heal (CTH) strategy.38-40 Although most SMVs exhibit low electrical conductivity, it can be increased rapidly in a moisture environment with high concentrations of carbon dioxide (CO₂),⁴¹ if the SMVs are hydrophilic. Therefore, by simply changing the humidity and the concentration of carbon dioxide on the surface of the hydrophilic SMV supporting material, different electrical conductivities can be obtained. Coupled with the different phase transition temperatures by infiltrating different PCMs, the form-stable PCM composites satisfy the requirement for different electrical conductivities and different phase transition temperatures. As a result, we hypothesize that electricity can be generated by directly connecting the two PCM composites based on the Seebeck effect.

This idea can be further explained as follows. It is known that ions in aqueous solution can move from the hot side to the cold side in a medium in the presence of a temperature gradient.42 The ion diffusion ability at the hot side is higher than that at the cold side. The ion movements cause an ion concentration gradient, which produces a potential difference. Therefore, we propose this new idea of obtaining electrical energy by merely using two types of SMV supported PCM composites. Although the dissolving ability of CO2 is decreased at higher temperatures, both ionization of carbonic acid and ion diffusivity are increased rapidly to speed up the ion movements from the hot side to the cold side. The increase in ion concentration at the cold side promotes the generation of carbonic acid and recombination into CO2. In a word, the CO2 enters the hot side, decomposes into ions, moves to the cold side, and recombines into CO2. Therefore, the greenhouse gas is only used as a medium to produce electricity. This idea does not reduce the emission of greenhouse gases, nor does it increase the greenhouse gas emission. The working principle is further illustrated in Fig. S1 in the ESI.†

To produce a continuous electricity output, we will use lighton and light-off cycles to maintain a constant temperature gradient between the two SMV-supported PCM composites. The reason is that during the light-on process, both the PCMs change from a solid to a liquid, absorbing a large amount of heat, but almost keeping the temperature at their corresponding phase transition temperature, thus maintaining a constant thermal gradient, which is one critical requirement for the Seebeck effect. To maintain a continuous electricity output, a light-off process must follow. During light-off, the two PCMs change from a liquid to a solid, which releases heat, but almost maintains a constant thermal gradient, again satisfying the requirement for the Seebeck effect. This light-on/-off process completes one cycle. The subsequent cycles will repeat the first cycle, *i.e.*, a light-on branch, followed by a light-off branch. As a result, a continuous and constant temperature gradient will be maintained, leading to continuous electricity production.

In this study, polyethylene glycol (PEG) and 1-tetradecanol (1-TD) are utilized as two types of pure PCMs. The SMV container, which is a rectangular hollow box, is obtained by 3D printing using a digital light processing (DLP) type of 3D printer. The two types of PCM composites are then connected with each other and water is sprayed on their surfaces. With different concentrations of carbon dioxide dissolved in the water, which is provided from a CO₂ storage tank, different electrical conductivities between the two sides of the PCM composites can be created, as shown in Fig. 1. In the following sections, we will report the preparation and test results of the new energy harvesting device.

2. Results and discussion

2.1 Morphologies of the synthesized shape memory vitrimer

Fig. S5a and b† show the FTIR peaks of diphenyl carbonate and di(trimethylolpropane) which were utilized as monomers to synthesize the SMV. The C=O peak of the diphenyl appears at 1750 cm⁻¹, and the peaks corresponding to the aromatic structure are observed close to 3000 cm⁻¹. The C-O peak of di(trimethylolpropane) is detected at 1000–1150 cm⁻¹, which indicates the intrinsic structure before the synthesizing process. The tris(2-aminoethylamine) (TREN) result is shown in Fig. S5c† and the initial tris[2-(acryloyloxy)ethyl] isocyanurate (TAI) chemical structure is shown in Fig. 2a. There are representative peaks of functional groups such as amide, C=O, and C=C that

would be crosslinked to a network structure. The TAI only 3D printed pre-vitrimer result is shown in Fig. S5d.† The TAI prepolymer synthesized from the two monomers exhibited different absorption peak intensities, as shown in Fig. S5e.† After 3D printing, the peak of the final SMV is presented in Fig. 2b. The -CH peak intensity is increased during the curing process. This indicates that the TAI pre-polymer synthesized from diphenyl carbonate and di(trimethylolpropane) is polymerized into a crosslinked SMV structure. To verify the chemical stability at different temperatures, Fig. S5f[†] shows the FTIR result, and there is no chemical reaction from 25 °C to 80 °C. To further demonstrate the synthesis of the SMV by the two monomers, the XPS measurement result is provided. Fig. S6a and b† show the results of diphenyl carbonate while Fig. S6c and d† show the results of di(trimethylolpropane). After crosslinking these two monomers, the structure is changed, as shown in Fig. S7.† The N 1s peak in Fig. S7c† indicates that the diphenyl carbonate and di(trimethylolpropane) are crosslinked by TREN effectively. The results of the final 3D printed SMV are presented in Fig. S8.† All generated functional groups exhibit C 1s and N 1s peaks. In addition, the atomic spectrum of the final SMV is shown in Fig. S8d† and nitrogen is increased significantly compared with that in the pre-polymer as shown in Fig. S7d.† The fabricated SMV exhibits an amorphous structure which is confirmed by the results of Raman peaks as shown in Fig. S9.† To compare the TAI only 3D printed pre-polymer and the synthesized SMV, TGA was performed and the results are shown in Fig. 2c; the characteristics are listed in Table 1. It is observed that the synthesized final SMV exhibits better thermal stability than the pre-vitrimer. The stress-strain behaviors are shown in Fig. S10a.† The tensile strength of the SMV is close to 10.0 MPa while that of the pre-vitrimer merely stops at 4.8 MPa.

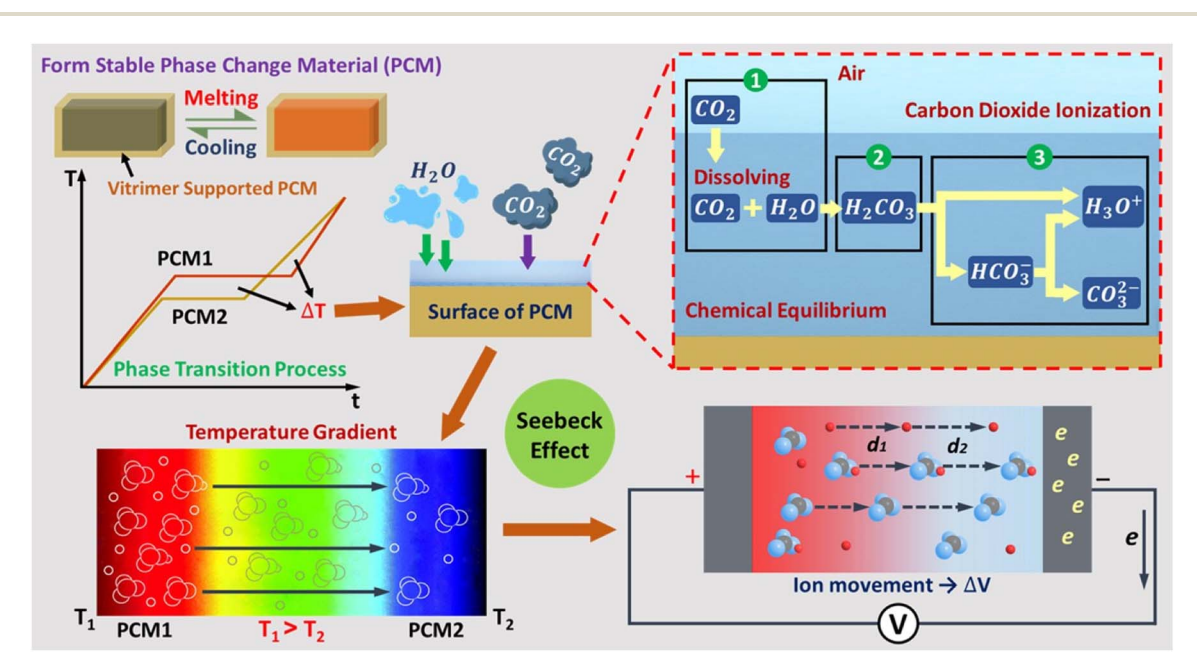


Fig. 1 Schematics of thermoelectric energy harvesting during the PCM phase transition process. Carbon dioxide (CO_2) can dissolve into the water to generate hydrogen, bicarbonate, and carbonate ions to promote the electrical properties. Definitely, the different CO_2 concentrations lead to various results of electrical energy harvesting during the light-on/-off process.

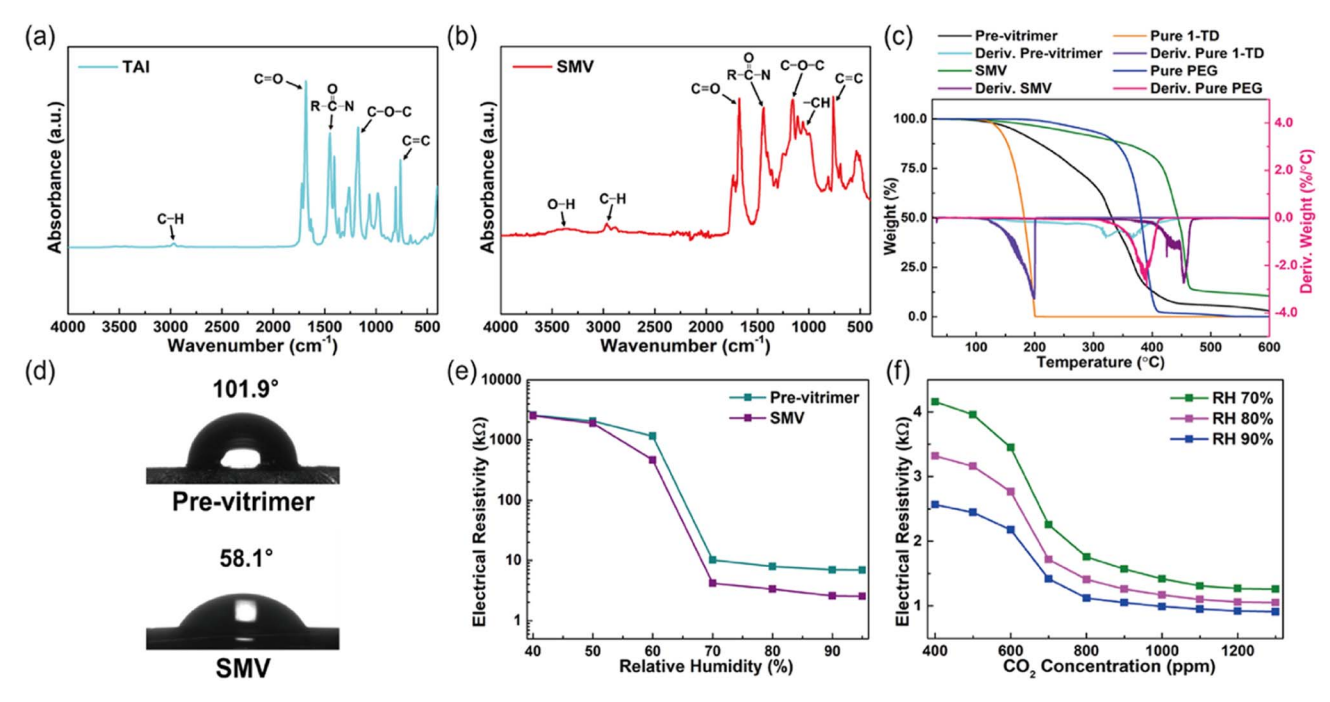


Fig. 2 FTIR results of (a) TAI and (b) final shape memory vitrimer (SMV). (c) TGA peaks of SMVs and pure PCMs. (d) Contact angle results of the pre-vitrimer and final SMV. (e) Electrical resistivity curves of the pre-vitrimer and final SMV with the increase in RH at the initial CO_2 concentration. (f) Electrical resistivity peaks of SMVs at RH 70%, 80%, and 90% which are flexible with the change in CO_2 concentration.

 $\mbox{{\bf Table 1}}\ \mbox{{\bf TGA}}$ data of pre-vitrimer, SMV, and pure PCMs under a $\mbox{{\bf N}}_2$ atmosphere

Samples	Onset (°C)	Peak (°C)	Endset (°C)	Residual mass (%)
Pre- vitrimer	121.08	378.65	448.26	3.05
SMV	203.81	452.37	475.24	10.60
Pure 1-TD	148.40	191.52	202.03	0.06
Pure PEG	218.66	385.94	411.58	0.15

Both the TGA and stress-strain results demonstrate that the synthesized SMV has excellent thermal and mechanical properties and is suitable for being utilized as a supporting material to fabricate the form-stable PCM composite.

Fig. 2d shows the contact angle measurement. The synthesized SMV is hydrophilic due to the incorporation of hydrogen functional groups. It can be concluded that the final SMV can easily absorb moisture and dissolve CO_2 from the environment. The surface structure of the SMV was obtained from the SEM images, as shown in Fig. S10b.† The SMV shows a flat surface structure while 1-TD and PEG contain a lot of wrinkles as presented in Fig. S10c and d.†

The result of electrical resistivity with the increase in external relative humidity (RH) is shown in Fig. 2e. It is seen that the electrical resistance of the SMV decreases rapidly at RH 70% (the initial RH in air is 40%). Furthermore, the electrical resistivity of the SMV can be decreased further with the increase in $\rm CO_2$ concentration (the initial $\rm CO_2$ concentration in air is 400 ppm), as shown in Fig. 2f. The electrical resistivity of the SMV is

decreased from 4.16 k Ω at 40% RH to 1.27 k Ω at RH 70%. At RH 80%, the electrical resistivity is changed from 3.32 k Ω to 1.06 k Ω , while it is changed from 2.57 k Ω to 0.92 k Ω under the RH 90% condition. It is easy to confirm that the electrical resistivity is difficult to decrease with the increase in temperature or CO₂ concentration at the initial RH of 40%, as shown in Fig. 3a–3c. One of the key points is that the CO₂ dissolving ability decreases with the increase in external temperature as indicated in Fig. 3d.⁴³ In this work, a RH of 70%, 80%, and 90% was utilized and the 400 ppm, 700 ppm, and 1200 ppm CO₂ concentrations were used to achieve electrical energy harvesting using the form-stable 1-TD and PEG composites during the light-on/-off process.

2.2 Thermal and form stabilities of PCM composites

Fig. 4a shows the UV-vis peaks of the pre-vitrimer and SMV with different thicknesses. It is obvious that all SMVs can transmit sunlight. As a result, the sunlight can pass through the SMV container and cause the phase transition process in the PCMs inside. Thermal stability is important for the supporting material to maintain an initial solid state without damage. The temperature sweep result is reported in Fig. 4b. Both the storage modulus and loss modulus decreased rapidly when the temperature was over 65 °C, and the maximum tan delta appeared at 70 °C. This indicated that the glass transition temperature (T_g) was close to 70 °C, and the SMV became flexible above 70 °C. Therefore, the thermal reliability tests for the two kinds of supporting materials were conducted with the change in external temperature from 25 °C to 80 °C. After several thermal cycles, the SMV supporting material retained

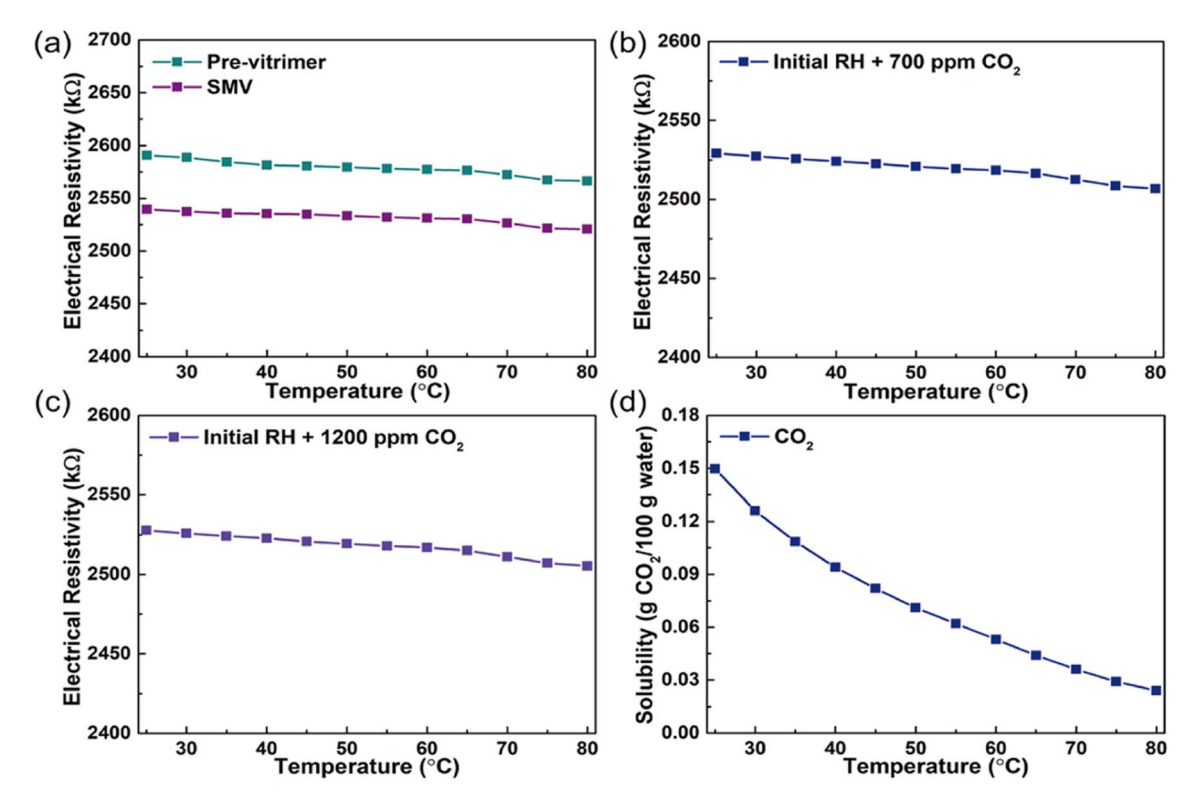


Fig. 3 Electrical resistivity of the (a) pre-vitrimer and final SMV, (b) initial RH at 700 ppm CO_2 concentration, (c) initial RH at 1200 ppm CO_2 concentration, and (d) CO_2 dissolving ability based on the temperature variation.

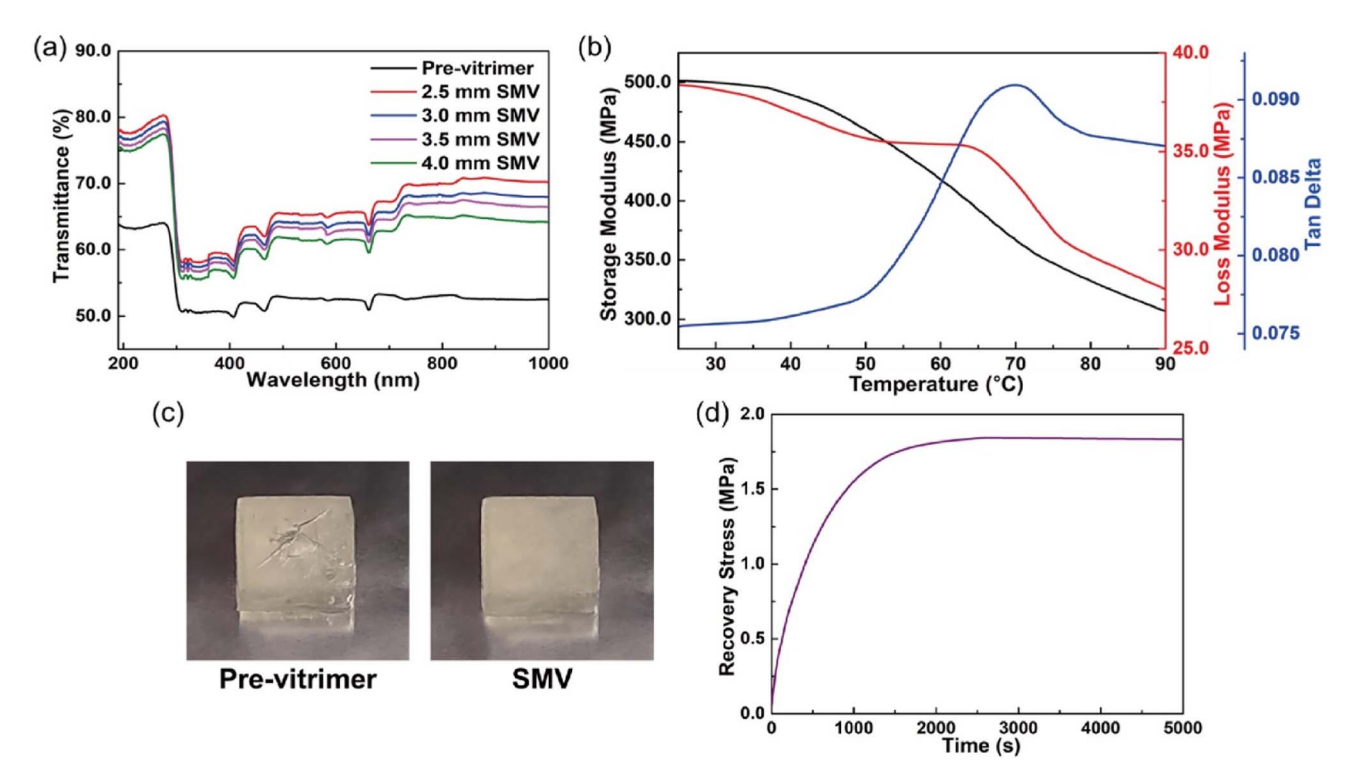


Fig. 4 (a) UV-vis peaks of the pre-vitrimer and SMV with different thicknesses. (b) Result of the SMV temperature sweep. (c) Form stability photo images of the pre-vitrimer and SMV after the light-on/-off process. (d) Recovery stress of SMV at 90 °C.

the initial shape successfully while the pre-vitrimer surface was fractured as shown in Fig. 4c. It was illustrated that the SMV supporting material exhibited great flexibility and thermal stability to prevent damage when subjected to thermal cycles. To demonstrate the shape memory effect of the SMV sample, the rectangular-shaped specimen was placed in a MTS chamber to undergo a hot programming process. The temperature of the MTS chamber was increased to 150 °C and was maintained to achieve a thermal equilibrium state. Then the specimen was compressed at a loading rate of 0.20 mm min⁻¹ until 13% strain. The cooling and unloading processes were followed to complete the whole compression programming process.⁴⁴ Eqn (1) and (2) are used to calculate the shape fixity ratio $R_{\rm f}$ and shape recovery ratio $R_{\rm r}$, respectively:

$$R_{\rm f} = \frac{\varepsilon_{\rm f}}{\varepsilon_{\rm l}} \times 100\% \tag{1}$$

$$R_{\rm r} = \frac{\varepsilon_{\rm l} - \varepsilon_{\rm t}(N)}{\varepsilon_{\rm l} - \varepsilon_{\rm t}(N - 1)} \times 100\% \tag{2}$$

where $\varepsilon_{\rm f}$ is the fixed strain after removing the load and $\varepsilon_{\rm l}$ is the strain before load removal. $\varepsilon_{\rm t}(N)$ and $\varepsilon_{\rm t}(N-1)$ are the final strains of the samples with a shape memory effect above the glass transition temperature $(T_{\rm g})$. For total recovery, $\varepsilon_{\rm t}(N-1)$ is eliminated when the N=1 ($\varepsilon_{\rm t}(0)$ equals 0).⁴⁵

The results of the shape fixity ratio $R_{\rm f}$ and shape recovery ratio $R_{\rm r}$ are listed in Table 2. The SMV showed excellent shape recovery properties and it can contribute to retain the high thermal stability without damage. Based on the close-then-heal (CTH) strategy, ⁴⁶ recovery stress plays an important role in bringing fracture surfaces in touch. Therefore, a recovery stress test was conducted. The compression programmed SMV sample was placed back into the MTS chamber, and the recovery test was started. Fig. 4d shows the SMV recovery stress at 90 °C as a function of time. It was found that the maximum stress was 1.84 MPa, which is sufficient to close micro-scale fatigue cracks. ⁴⁷ Therefore, the SMV can heal the potential fatigue cracks under cyclic thermal loading.

To confirm the form stability of the SMV supported PCM composites, optical images of the pure PCM and PCM composites were obtained, which demonstrated the form stabilities, as shown in Fig. S11.† This indicates that both the pure 1-TD and PEG were fully melted into a liquid state at 80 °C. The different sizes of the SMV supported PCM composites maintained the initial solid state without any leakage during the melting process. The volume expansion results of the PCM composites are shown in Fig. S12a and b.† The different sizes of the SMV containers merely exhibit a slight volume expansion especially for the 3.5 mm and 4.0 mm thick specimens. The

Table 2 Shape fixity ratio (R_f) and shape recovery ratio (R_r) of the SMV

Samples	Shape fixity ratio (R_f)	Shape recovery ratio (R_r)
Pre-vitrimer		—
SMV	91.93%	99.00%

thermal conductivity measurement was conducted and that of both the SMV supported 1-TD and PEG composites was close to 0.33 W mK⁻¹ as indicated in Fig. S12c.† Definitely, the thermal conductivity of the PCM composites was mainly correlated with the SMV container. Fig. S12d† shows the XRD peaks of the SMV, pure PCMs, and PCM composites. Only intrinsic crystal peaks appear, which confirms that no chemical reaction occurred between the SMV and pure PCMs. To verify the temperature gradients during the light-on/-off process, the IR camera images were obtained as shown in Fig. 5. The temperature of the SMV container was changed rapidly while the SMV supported 1-TD and PEG composites underwent almost isothermal phase transition. From Fig. 5b and c, it is seen that the SMV supported PEG and 1-TD composites underwent a nearly isothermal process within a certain period of time (a section of the temperature-time curve is almost a horizonal line), which is the phase transition period of each PCM. It is also seen that the period of time corresponding to the isothermal process for these two composites is different, suggesting that a certain temperature gradient can be maintained to trigger the Seebeck effect. The DSC results of the SMV and pure PCMs demonstrated the phase change temperature and latent heat (ΔT) properties, as shown in Fig. S13.† The PEG had higher melting and cooling points $(T_{\rm mp}, T_{\rm cp})$ than those of 1-TD, as shown in Fig. S13b and c.† From Fig. S13a,† it is seen that the SMV is also stable after 100 thermal cycles. The stability under thermal cycles of the SMV, 1-TD, and PEG can be further validated by using Fig. S13d.† Furthermore, the DSC cycling results are listed in Table S2.† It is seen that there is only a slight difference after completing 100 heating/cooling cycles, suggesting that the composite assembly is stable.

The SMV supported PCM composites maintain excellent thermal and chemical stabilities during the thermal cycling test, which is also validated by the XRD peaks as shown in Fig. S13d.† Therefore, the SMV container can support the pure 1-TD and PEG to fabricate form-stable PCM composites, which can be further utilized in smart and controllable energy harvesting.

2.3 Electrical energy harvesting under different conditions

The sunlight intensity on the surface of the PCM composites was defined as 15 mW cm⁻² which exhibited appropriate electrical energy harvesting during the light-on/-off process.48 The final temperatures of the SMV with different RHs are shown in Fig. S14a.† It is clear that the SMV can reach 81 °C within the range of RH from 40% to 90%. Under the initial air conditions with 400 ppm CO₂, the electrical resistivity of the SMV was gradually increased during the light-on heating process. The decrease in CO2 dissolving ability caused the low ion concentration in moisture at different RHs as shown in Fig. S14b-d.† However, after increasing the CO₂ concentration to 700 ppm, the electrical resistivity became lower than that in the initial state as shown in Fig. S15a-c.† At the highest CO2 concentration of up to 1200 ppm, the electrical resistivity was a little lower than that at the 700 ppm concentration level due to the dissolution of additional CO₂ as shown in Fig. S15d-f.† Thus, the

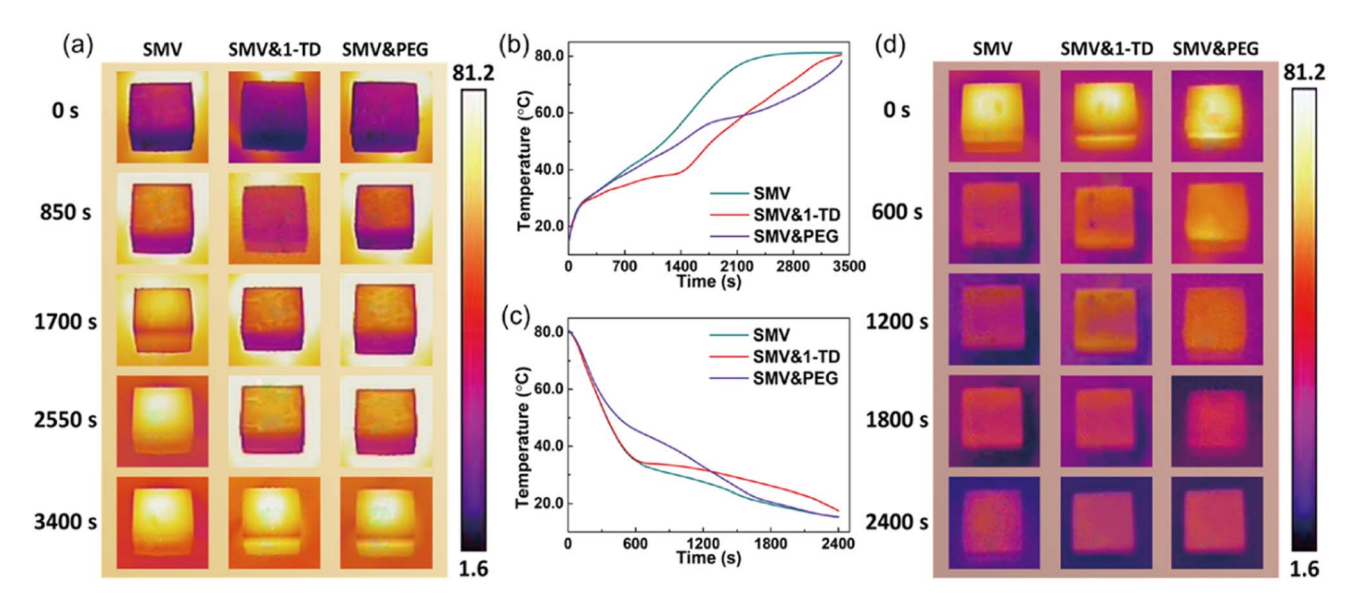


Fig. 5 (a) IR camera temperature gradient of SMV and SMV supported PCM composites during the light-on process. (b) Temperature peaks during the light-on process. (c) Temperature peaks during the light-off process. (d) IR camera temperature gradient of SMV and SMV supported PCM composites during the light-off process.

700 ppm and 1200 ppm CO₂ concentrations can provide a good external environment to make a conductible SMV structure. Fig. S16† shows the electrical resistivity of the SMV supported 1-

TD and PEG composites with different SMV container sizes under RH 70% conditions. Both the SMV supported 1-TD and PEG composites merely exhibited a slight difference within the

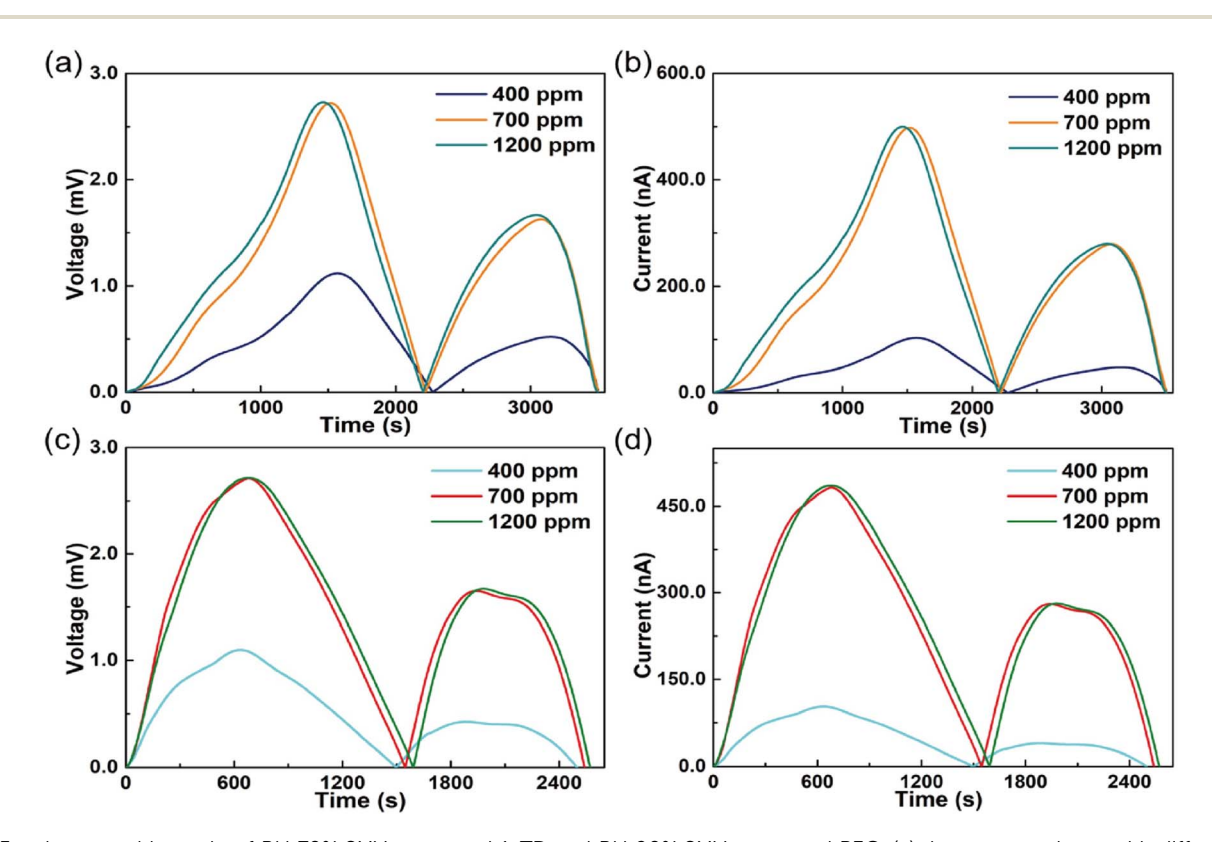


Fig. 6 For the assembly made of RH 70% SMV supported 1-TD and RH 90% SMV supported PEG, (a) the output voltage with different CO_2 concentrations during the light-on process and (b) output current with different CO_2 concentrations during the light-on process. (c) Output voltage with different CO_2 concentrations during the light-off process and (d) output current with different CO_2 concentrations during the light-off process.

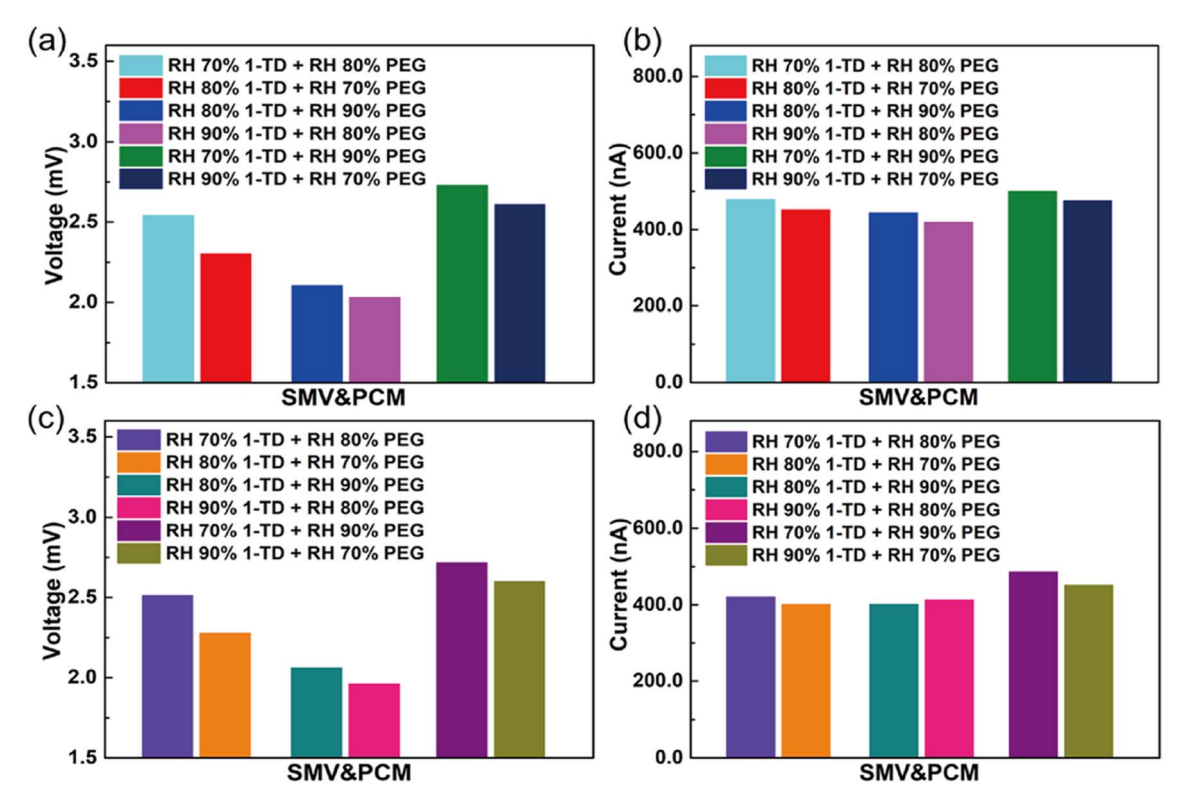


Fig. 7 For the light-on/-off process with different CO_2 concentrations, (a) the maximum output voltage during the light-on process and (b) the maximum output current during the light-on process. (c) The maximum output voltage during the light-off process and (d) the maximum output current during the light-off process.

range of CO₂ concentration from the initial 400 ppm to 1200 ppm. The electrical resistivity at RH 80% and 90% is similar as shown in Fig. S17 and S18,† respectively. However, the PCM has an optimum volume size in order to effectively transfer the stored thermal energy to electrical energy during the phase transition process. 49 To find out the optimum size of the SMV supported PCM composites, the temperature variation test was conducted and Fig. S19† shows the result of different sizes of the 1-TD composite at different CO₂ concentrations. It is clear that the 2.5 mm and 3.0 mm thick SMV container supported 1-TD composites exhibit a lower phase transition field. The 3.5 mm and 4.0 mm thick SMV supported 1-TD composites exhibited a similar result at 400 ppm, 700 ppm, and 1200 ppm CO₂ concentrations. On the other hand, the 3.5 mm thick SMV supported PEG composite exhibited the most appropriate temperature peaks as shown in Fig. S20.† Based on the results of temperature peaks, the 3.5 mm thick SM supported 1-TD and PEG composites were selected to generate electrical energy at different RH and CO2 concentrations.

Fig. S21† shows the temperature peaks of the 1-TD composite at the three different CO_2 concentrations during the light-on/-off process. The CO_2 concentration changes from the initial 400 ppm to 1200 ppm, and the heating rate was increased in the light-on heating process while the cooling rate was decreased due to the CO_2 greenhouse effect. The PEG composite had the same effect as the 1-TD composite in the same range of RH and CO_2 concentrations, as shown in Fig. S22.†

To observe the electrical energy output during the light-on/off process, different CO2 concentrations were utilized at the initial RH 40%. No voltage and current were produced as presented in Fig. S23.† The change in the RH on one side, as shown in Fig. S24 and S25† during the light-on/-off process, merely illustrated the noise effect. Based on the above test, the RH at each side of the PCM composite assembly should be over 70% to decrease the electrical resistivity of the SMV structure. Therefore, RH 70% was used on the 1-TD composite side and RH 80% was used on the PEG composite side to generate electrical energy. The results are shown in Fig. S26.† Both the output voltage and current at the initial 400 ppm were lower than those at 700 ppm and 1200 ppm CO₂ concentrations during the light-on/-off process. The first cycle of voltage and current appeared up to 2300 s due to the temperature difference between the 1-TD and PEG composites. After the 1-TD composite completed the phase transition process, the temperature profile was reversed when the PEG composite underwent a phase transition. The second peak lasted for 3500 s and the output current was lower than that in the 1st cycle because the high temperature decreased the CO2 dissolving ability. In contrast, the output voltage and current were produced rapidly due to the natural cooling during the light-off process. The 1st cycle was terminated at 1500 s and the energy harvesting was maintained over 2500 s at 700 ppm and 1200 ppm CO₂ concentrations. Compared with the light-on process, the 2nd cycle current peaks during the light-off

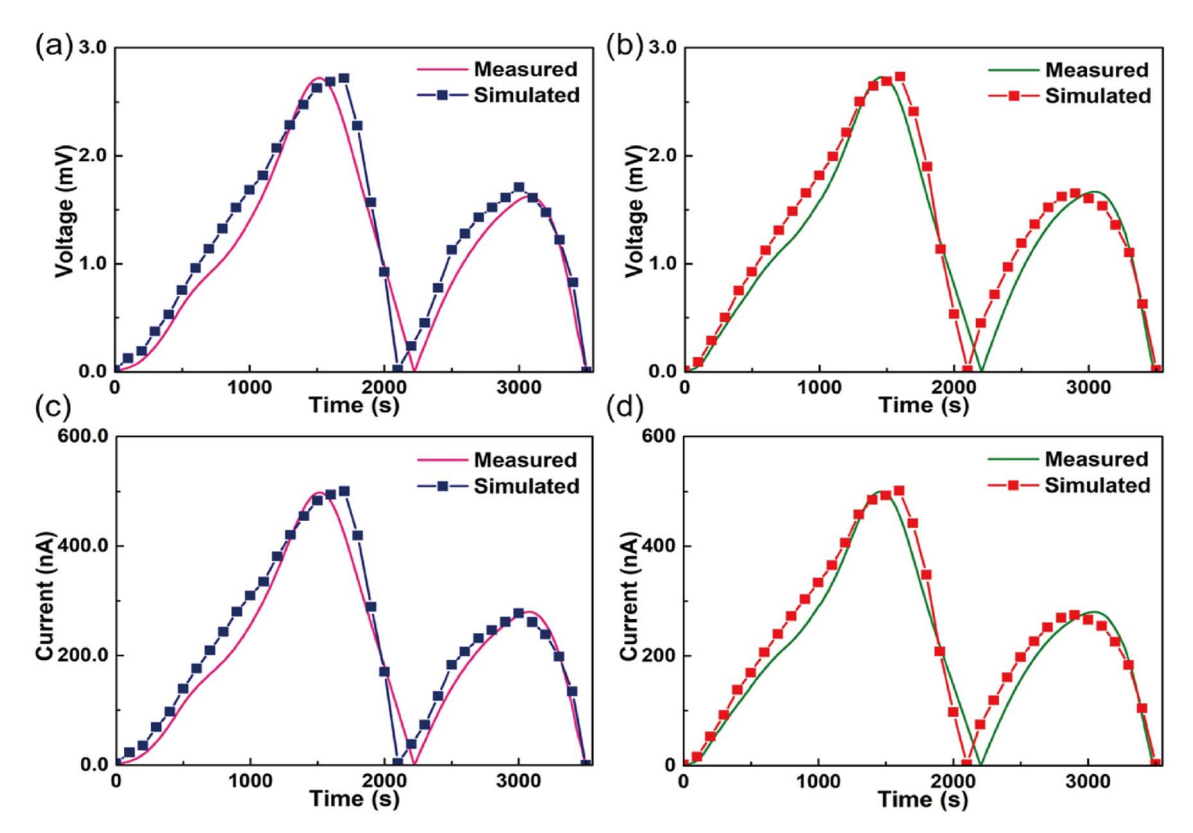


Fig. 8 For the assembly made of RH 70% SMV supported 1-TD and RH 90% SMV supported PEG, the comparison with simulated profiles during the light-on process, (a) output voltage at 700 ppm CO₂ concentration and (b) output voltage at 1200 ppm CO₂ concentration. (c) Output current at 700 ppm CO₂ concentration and (d) output current at 1200 ppm CO₂ concentration.

process were higher because the CO₂ dissolving ability was increased on cooling. The output current was shifted a little due to the change in electrical resistivity with change in external temperature. The maximum voltage and current were approximately 2.54 mV and 477.83 nA, respectively. Furthermore, the long-term durability test was conducted to demonstrate the repeatability at 700 ppm and 1200 ppm ${\rm CO_2}$ concentrations as shown in Fig. S27 and S28,† respectively. The second assembly was prepared using the RH 80% 1-TD composite and RH 70% PEG composite. Fig. S29† shows the results of voltage and current output during the light-on/-off process, and the cycling results of energy harvesting are presented in Fig. S30 and S31.† The maximum voltage and current were close to 2.30 mV and 450.80 nA, which were lower than those in the first assembly. Basically, the PEG composite acted as the hot side of the PCM device due to the higher phase transition temperature than that of the 1-TD composite. This indicated that the high concentration of CO₂ at the hot side of the PCM device can increase the power output during the light-on/-off process. When the RH was over 80%, Fig. S32-S34† show the assembly made of the RH 80% 1-TD composite and RH 90% PEG composite. The high RH led to a decrease in the electrical resistivity, although the voltage and current outputs were even lower than those in the second assembly. The maximum voltage was close to 2.10 mV and the current was 443.00 nA under high RH conditions. The RH 90% 1-TD composite and RH 80% PEG composite assembly was

selected to generate electrical energy and the results are shown in Fig. S35.† Fig. S36 and S37† exhibit the repeatable energy harvesting. The maximum voltage was 2.03 mV with 418.70 nA current output which exhibited lower efficiency for energy harvesting. Therefore, the concept of the Seebeck effect for energy harvesting requires an appropriate difference in electrical resistivity between the two sides of the materials. High RH with low electrical resistivity led to a relatively low difference in electrical resistivity between 1-TD and PEG composites. As a result, increasing the difference between electrical resistivity was a key factor to improve the energy harvesting efficiency. Based on the above test results, the RH 70% 1-TD composite with the RH 90% PEG composite was utilized to observe the voltage and current output, and the results are shown in Fig. 6. It is easy to find out that the voltage and current outputs were higher than those in the previous assembly and the maximum voltage and current were 2.73 mV and 500.00 nA, respectively. Fig. S38 and S39† show the stable long-term durability during the phase transition process. Even with the change in RH between the 1-TD and PEG composites, the maximum voltage was close to 2.61 mV and the current was 474.60 nA as presented in Fig. S40-S42.† Based on the output power test, the optimum external condition was defined as an assembly made of the RH 70% 1-TD composite connected with the RH 90% PEG composite.

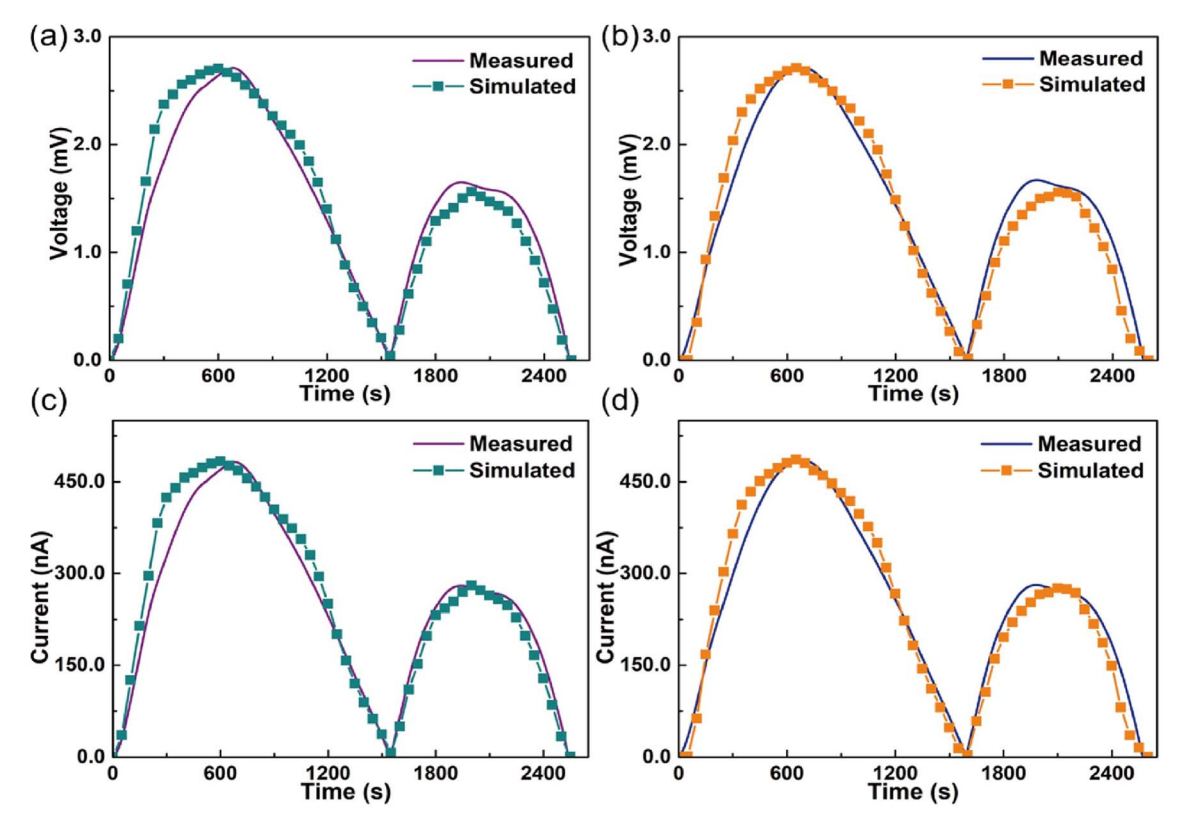


Fig. 9 For the assembly made of RH 70% SMV supported 1-TD and RH 90% SMV supported PEG, the comparison with simulated profiles during the light-off process, (a) output voltage at 700 ppm CO_2 concentration and (b) output voltage at 1200 ppm CO_2 concentration. (c) Output current at 700 ppm CO_2 concentration and (d) output current at 1200 ppm CO_2 concentration.

2.4 Energy harvesting results by comparison with numerical simulations

To find out the maximum voltage and current outputs during the light-on/-off process, Fig. 7 shows the results of the PCM composites with different RHs during the change in CO₂ concentrations. Based on the maximum voltage and current of 2.73 mV and 500.00 nA during the light-on process, the maximum outputs were 2.72 mV and 485.69 nA during the lightoff process, which were higher than those in previous research using a similar concept.50 This demonstrated that the assembly with the RH 70% 1-TD composite and RH 90% PEG composite exhibited excellent electrical energy harvesting ability at 700 ppm and 1200 ppm CO₂ concentrations during the lighton/-off process. To obtain the temperature profiles at 700 ppm and 1200 ppm CO₂ concentrations, Fig. S43† shows the results of the temperature curves during the light-on/-off process. The rate of temperature change was increased at the 1200 ppm level as shown in Fig. S43a† while the opposite result during the light-off process as shown in Fig. S43b.† The output voltage was correlated with the temperature difference between the two sides of the PCM composites. Fig. S44a and b† show the comparison between the measured temperature and the simulated result. It is clear that the numerical profiles are in agreement with the experimental peaks, which means the experimental results were correct during the light-on/-off process. Fig. 8 shows the results of the voltage and current at 700 ppm and 1200 ppm by comparison with the numerical

simulations. The maximum voltage and current were identical, and the assembly made of the RH 70% 1-TD composite and RH 90% PEG composite led to effective electrical energy harvesting. Fig. S44c and d† show the comparison between the experimental and numerical peaks. There are no obvious differences at the 700 ppm and 1200 ppm CO₂ concentrations during the light-off process. In addition, the experimental voltage and current peaks were quite in agreement with the numerical simulation results as shown in Fig. 9, which demonstrates that the SMV supported PCM composites can generate stable and continuous electrical energy during the light-on/-off process. The electrical energy harvesting efficiency is presented in Fig. S44e† and the light-on heating and light-off cooling efficiencies were approximately 61.88% and 49.76%, respectively, at the 700 ppm CO₂ concentration. Furthermore, the PCM composites at the 1200 ppm CO₂ concentration showed 61.76% and 49.14% efficiencies during the light-on/-off process. To summarize the experimental and numerical results, high RH at 700 ppm and 1200 ppm CO₂ concentrations can produce an electrical resistivity difference and harvest electrical energy during the PCM phase transition process.

3. Conclusions

In this work, we successfully synthesized a shape memory vitrimer (SMV) and 3D printed SMV hollow containers as a supporting material for the preparation of a form-stable phase

change material (PCM) composite. Both 1-tetradecanol (1-TD) and polyethylene glycol (PEG) infiltrated SMV containers exhibited excellent form-stability during the melting process of the PCMs without any leakage. Electrical energy harvesting was achieved by merely connecting the two different PCM composites. The energy harvesting efficiency was increased by changing the relative humidity (RH) and carbon dioxide (CO₂) concentrations on the surface of the SMV containers. This was an unprecedented discovery in the energy harvesting research area by using form-stable PCM composites during the light-on/-off process. It was found that high RH conditions promoted the dissolving ability of CO2, and the electrical resistivity was decreased significantly. Although the CO2 dissolving ability changed based on the temperature variation, the difference in electrical resistivity between the two sides of the PCM composite can induce the Seebeck effect and produce electrical energy during the light-on/-off process. It was found that the power output was decreased at high RH and high CO₂ concentration due to the similar electrical resistivity on the two sides of the composites. To overcome this problem, the assembly made of RH 70% 1-TD and RH 90% PEG composites were employed and obtained the highest voltage and current outputs up to 2.73 mV and 500 nA, respectively. The PCM composites showed high energy harvesting efficiency at 700 ppm and 1200 ppm CO2 concentrations which indicated that greenhouse gases can be utilized to help harvest energy. This has high potential for application in industry, vehicles, aerospace, households, and agriculture to produce a large amount of electrical energy from solar energy simply and easily.

It is noted that the use of CO_2 is to demonstrate that a greenhouse gas can be utilized to do something good. The concept proposed in this study, however, is general. Other organic or inorganic compounds, whether solids, liquids, or gases, can also be employed as long as they can be dissolved in water to produce ions.

4. Experimental section

4.1 Materials

Diphenyl carbonate, di(trimethylolpropane), tris(2-aminoethylamine), dichloromethane, tris(2-(acryloyloxy)ethyl) isocyanurate (TAI), diphenyl(2,4,6-trimethylbenzoyl)phosphine oxide (TPO), 1-tetradecanol (1-TD), and polyethylene glycol (PEG, Mn = 6000) were purchased from Sigma-Aldrich.

4.2 Preparation of the shape memory vitrimer supporting material

The first step to fabricate a shape memory vitrimer (SMV) supporting material was to mix 90.0 g diphenyl carbonate with 21.0 g di(trimethylopropane) in a 140 $^{\circ}$ C oil bath for 2 hours. After this, 0.6 g tris(2-aminoethylamine) was dissolved in 6.50 mL dichloromethane (CH₂Cl₂), and was poured into the melted mixture which acted as a cross-linking agent to cause the polymerization reaction as shown in Fig. S2.† The pre-polymer was added to tris(2-(acryloyloxy)ethyl) isocyanurate (TAI) at a 120:90 mass ratio and stirred for 5 minutes. 9.0 g photo-initiator diphenyl(2,4,6-

trimethylbenzoly)phosphine oxide (TPO) was then added to the polymer mixture. After this, the mixture was placed in an oven at 120 $\,^{\circ}$ C for 30 minutes. The melted solution was then taken out and stirred for 1 hour with a stirring bar (at 500 rpm) and cooled down to room temperature in 30 minutes. As shown in Fig. S3,† the pre-polymer was placed in a 3D printer. The SMV hollow box with a dimension of 20 mm \times 20 mm \times 2.5 mm was printed by the 3D printer. To compare the mechanical and hydrophilic properties of the synthesized SMV, a hollow box container was also printed by using TAI only, which was labeled as the previtrimer. To confirm the optimum thickness of SMV containers, four different container thicknesses were fabricated and labeled as 2.5 mm, 3.0 mm, 3.5 mm, and 4.0 mm.

4.3 Preparation of SMV supported form-stable PCM composites

Fig. S4a† shows the fabrication route of the form-stable PCM composite. The 3D printed SMV container has a 1 mm edge thickness which can prevent pure PCM from leaking. Pure 1-TD and PEG were melted to a liquid state and poured into two SMV containers until full. The pre-polymer (pre-SMV) was painted onto two surfaces of the SMV containers, and they were pushed into contact. The assembly was then placed in an ultraviolet (UV) chamber. After 80 seconds of UV curing treatment, a formstable SMV supported PCM composite device was fabricated successfully. To determine an appropriate size of the PCM composite device, the SMV containers with four different sizes, as shown in Fig. S4b,† were utilized to fabricate the SMV supported 1-TD and PEG composites. The weight of the SMV container and PCM composites are listed in Table S1.† To verify the electrical resistivity with the change in external relative humidity (RH) and carbon dioxide (CO₂) concentrations, the initial state of RH 40% with 400 ppm CO2 was changed gradually by increasing both the RH and CO₂ concentration.

4.4 Characterization

Fourier transform infrared spectroscopy (FTIR, Spectrum Two, PerkinElmer, MA, USA) was utilized to observe the chemical functional groups of the monomers and final SMV. The surface structures of the SMV and phase change materials (PCMs) were obtained by using a field emission scanning electron microscope (FE-SEM, Quanta 3d FEG Dual Beam, FEI, Hillsboro, USA) after platinum coating. The transmittance of SMVs with various thicknesses was measured using a UV-vis-NIR spectrophotometer in the 190-1000 nm wavelength range (UV-3600, Shimadzu, Kyoto, Japan). The typical crystal structures of the PCM composites were measured by X-ray diffraction (XRD, Panalytical Empyrean, Malvern, UK) in the range of 10-60° with a scan rate of 3° min⁻¹. The stress-strain and shape recovery behaviors of the SMV were determined by using a 2610 universal testing machine (UTM, Norwood, MA, USA). The sample dimensions for recovery stress were 10.34 mm imes 9.24 mm imes4.70 mm. A thermal gravimetric analyzer (TGA550, TA Instruments, DE, USA) was utilized to measure the thermal stabilities of SMV and pure PCMs. For the SMV supported form-stable PCM composites, a rheometer (HR30, TA Instruments, DE,

USA) was used to observe the volume expansion with temperature variation from 25 °C to the final 80 °C. To demonstrate the SMV structures which were synthesized by using monomers, Xray photoelectron spectroscopy (XPS, Scienta omicron, Uppsala, Sweden) and Raman spectroscopy (Renishaw Invia Raman Microscope, TX, USA) were used to confirm the intrinsic functional peaks. A contact angle analyzer (FTA1000, First Ten Angstroms, VA, USA) was utilized to investigate the hydrophilic ability of the SMV material. The thermal conductivities of the pure PCM and PCM composites were confirmed by using a thermal conductivity analyzer (C-Therm TCi, C-Therm Technologies Ltd, NB, Canada). The phase transition temperature and latent heat (ΔT) were obtained using differential scanning calorimetry (DSC4000, PerkinElmer, MA, USA) in the range of 0 °C to 90 °C at a scanning rate of 10 °C min⁻¹. The temperature gradients of the SMV supported PCM composites during the light-on/-off process were observed by using an IR highresolution thermal camera (B20, HIKMICRO, Hangzhou, China). The temperature change of the SMV supported PCM composites was measured by using a functional multi-meter (UT61, Guangdong, China), and the electrical energy output was recorded by using a source meter (SourceMeter2400, KEITHLEY, OR, USA).

Author contributions

Chengbin Yu: conceptualization; methodology; validation; investigation; writing-original draft preparation. John Konlan: validation. Guoqiang Li: supervision; funding acquisition; writing – revision & editing. All authors have read and agreed to the published version of the manuscript.

Conflicts of interest

The authors declare that they have no known competing financial interests or personal relationships that could have appeared to influence the work reported in this paper.

Acknowledgements

This work was funded by the US National Science Foundation under Grant Number OIA-1946231 and the Louisiana Board of Regents for the Louisiana Materials Design Alliance (LAMDA), the US National Science Foundation under grant number 1736136, and the US National Science Foundation under grant number 2051050. The authors would like to thank the Advanced Manufacturing and Machining Facility (AMMF) at Louisiana State University for providing the facilities to cut our samples. The authors also would like to thank Professor Qinglin Wu in the School of Renewable Natural Resources at Louisiana State University AgCenter for assisting in testing the contact angle.

References

1 K. K. Kurramovich, A. A. Abro, A. I. Vaseer, S. U. Khan, S. R. Ali and M. Murshed, *Environ. Sci. Pollut. Res.*, 2022, 1–20.

- 2 Y. Shang, L. Zhu, F. Qian and Y. Xie, *Renewable Energy*, 2023, 206, 890–896.
- 3 R. R. Hernandez, A. Armstrong, J. Burney, G. Ryan, K. Moore-O'Leary, I. Diédhiou, S. M. Grodsky, L. Saul-Gershenz, R. Davis and J. Macknick, *Nat Sustainability*, 2019, 2, 560–568.
- 4 X. Liu, Y. Yuan, J. Liu, B. Liu, X. Chen, J. Ding, X. Han, Y. Deng, C. Zhong and W. Hu, *Nat. Commun.*, 2019, **10**, 4767.
- 5 D. Fernández-González, I. Ruiz-Bustinza, C. González-Gasca, J. P. Noval, J. Mochón-Castaños, J. Sancho-Gorostiaga and L. F. Verdeja, Sol. Energy, 2018, 170, 520-540.
- 6 T. Ding, Y. Zhou, W. L. Ong and G. W. Ho, *Mater. Today*, 2021, 42, 178–191.
- 7 P. Denholm, Technical Potential of Solar Water Heating to Reduce Fossil Fuel Use and Greenhouse Gas Emissions in the United States, National Renewable Energy Lab.(NREL), Golden, CO (United States), 2007.
- 8 X. Jin, S. W. Leow, Y. Fang and L. H. Wong, *J. Mater. Chem. A*, 2023, **11**, 12992–12998.
- 9 A. K. Hamzat, M. I. Omisanya, A. Z. Sahin, O. R. Oyetunji and N. A. Olaitan, *Energy Convers. Manage.*, 2022, **266**, 115790.
- 10 X. Mu, J. Zhou, P. Wang, H. Chen, T. Yang, S. Chen, L. Miao and T. Mori, *Energy Environ. Sci.*, 2022, **15**, 3388–3399.
- 11 N. Sommerfeldt and J. M. Pearce, *Appl. Energy*, 2023, **336**, 120838.
- 12 C.-T. Hsu, G.-Y. Huang, H.-S. Chu, B. Yu and D.-J. Yao, *Appl. Energy*, 2011, **88**, 5173–5179.
- 13 Y. Gao, M. Zhang, Y. Cui, D. Bao, F. Xu, X. Shen, Y. Zhu and H. Wang, *J. Mater. Chem. A*, 2022, **10**, 10452–10465.
- 14 X. Zhang, B. C. Shiu, T.-T. Li, X. Liu, H.-T. Ren, Y. Wang, C.-W. Lou and J.-H. Lin, *Chem. Eng. J.*, 2021, **426**, 131923.
- 15 D. Liu, C. Lei, K. Wu and Q. Fu, ACS Nano, 2020, 14, 15738–15747.
- 16 W. Zhang, R. Mazzarello, M. Wuttig and E. Ma, *Nat. Rev. Mater.*, 2019, 4, 150–168.
- 17 Y. Zhang, J. Wang, J. Qiu, X. Jin, M. M. Umair, R. Lu, S. Zhang and B. Tang, *Appl. Energy*, 2019, 237, 83–90.
- 18 R. Gulfam, P. Zhang and Z. Meng, *Appl. Energy*, 2019, **238**, 582–611.
- 19 D.-C. Gao, Y. Sun, A. M. Fong and X. Gu, *Energy Storage Mater.*, 2022, **46**, 100–128.
- 20 B. Zivkovic and I. Fujii, Sol. Energy, 2001, 70, 51-61.
- 21 C. Yu and Y. S. Song, Compos. Commun., 2023, 40, 101600.
- 22 C. Yu, J. R. Youn and Y. S. Song, *Macromol. Res.*, 2019, 27, 606–613.
- 23 Y. Cao, Y. Meng, Y. Jiang, S. Qian, D. Fan, X. Zhou, Y. Qian, S. Lin, T. Qian and Q. Pan, *Chem. Eng. J.*, 2022, 134549.
- 24 D. Ghosh, J. Ghose, P. Datta, P. Kumari and S. Paul, *J. Energy Storage*, 2022, 53, 105179.
- 25 P. Yan, W. Fan, Y. Yang, H. Ding, A. Arshad and C. Wen, *Appl. Energy*, 2022, **327**, 120064.
- 26 H. Guo, W. Jiao, H. Jin, Z. Yuan and X. He, *Adv. Funct. Mater.*, 2023, **33**, 2209345.
- 27 Y. Chang, X. Yao, Y. Chen and D. Zou, *Composites, Part B*, 2023, 110584.
- 28 C. Yu, J. R. Youn and Y. S. Song, *Fibers Polym.*, 2020, **21**, 24–32.

- 29 L. Wang and D. Meng, Appl. Energy, 2010, 87, 2660-2665.
- 30 C. Yu and Y. S. Song, Nanomaterials, 2021, 11, 2192.
- 31 M. Zhou, D. Xie, K. Zhou, K. Gong, L. Yin, X. Qian and C. Shi, *Sol. Energy Mater. Sol. Cells*, 2022, **236**, 111537.
- 32 C. Yu and Y. S. Song, J. Energy Storage, 2023, 58, 106360.
- 33 C. Yu and Y. S. Song, Energy Technol., 2023, 11, 2201108.
- 34 Z. Niu and W. Yuan, ACS Sustain. Chem. Eng., 2019, 7, 17523–17534.
- 35 C. Yu, J. R. Youn and Y. S. Song, *Macromol. Res.*, 2021, 29, 534–542.
- 36 J. Konlan, P. Mensah, S. Ibekwe and G. Li, *J. Compos. Mater.*, 2022, **56**, 2267–2278.
- 37 F. Meng, M. O. Saed and E. M. Terentjev, *Nat. Commun.*, 2022, 13, 5753.
- 38 G. Li and D. Nettles, *Polymer*, 2010, **51**, 755-762.
- 39 L. Lu, J. Pan and G. Li, J. Mater. Chem. A, 2017, 5, 21505-21513.
- 40 X. Feng and G. Li, ACS Appl. Mater. Interfaces, 2020, 12, 57486–57496.

- 41 Z. Feng, W. Zhao, Z. Yang, Y. Deng, T. Yang and Y. Ni, *J. Mater. Chem. A*, 2022, **10**, 11524–11534.
- 42 L. Rezende Franco, A. L. Sehnem, A. M. Figueiredo Neto and K. Coutinho, *J. Chem. Theory Comput.*, 2021, 17, 3539–3553.
- 43 N. Abas and N. Khan, J. CO2 Util., 2014, 8, 39-48.
- 44 A. Li, J. Fan and G. Li, J. Mater. Chem. A, 2018, 6, 11479–11487.
- 45 P. Utroša, O. C. Onder, E. Žagar, S. Kovačič and D. Pahovnik, *Macromolecules*, 2019, 52, 9291–9298.
- 46 G. Li and N. Uppu, Compos. Sci. Technol., 2010, 70, 1419–1427.
- 47 A. Shojaei, S. Sharafi and G. Li, Mech. Mater., 2015, 81, 25-40.
- 48 C. Yu, H. Kim, J. R. Youn and Y. S. Song, *ACS Appl. Energy Mater.*, 2021, **4**, 11666–11674.
- 49 C. Yu, S. H. Yang, S. Y. Pak, J. R. Youn and Y. S. Song, *Energy Convers. Manage.*, 2018, **169**, 88–96.
- 50 C. Yu and G. Li, Energy Convers. Manage., 2024, 299, 117851.